Child abuse associates with increased recruitment of perineuronal nets in the ventromedial prefrontal cortex: evidence for an implication of oligodendrocyte progenitor cells

Arnaud Tanti[1,2], Claudia Belliveau[1,3], Corina Nagy[1], Malosree Maitra[1,3], Fanny Denux[1], Kelly Perlman[1,3], Frank Chen[1], Refilwe Mpai[1,3], Candice Canonne[1], Maria Antonietta Davoli[1], Gustavo Turecki[1,4] and Naguib Mechawar[1,4]

Affiliations

[1] McGill Group for Suicide Studies, Douglas Mental Health University Institute, Verdun, QC, Canada.

[2] Current address: UMR 1253, iBrain, Université de Tours, Inserm, Tours, France.

[3] Integrated Program in Neuroscience, McGill University, Montreal, QC, Canada.

[4] Department of Psychiatry, McGill University, Montreal, QC, Canada.

Corresponding author

Naguib Mechawar, PhD

McGill Group for Suicide Studies, Douglas Mental Health University Institute

Department of Psychiatry, McGill University

naguib.mechawar@mcgill.ca

Content

Main Text – Abstract, Introduction, Results, figure legends and discussion (1874 words)

Methods (1311 words)

2 figures, 1 table

15 references

Abstract

Child abuse (CA) is a strong predictor of psychopathologies and suicide, and can lastingly alter normal trajectories of brain development, in particular in areas closely linked to emotional responses such as the prefrontal cortex (PFC). Yet, the cellular underpinnings of these enduring effects are unclear. Childhood and adolescence are marked by the protracted formation of perineuronal nets (PNNs), which are essential in orchestrating the closure of developmental windows of cortical plasticity by regulating the functional integration of parvalbumin interneurons (PV) into neuronal circuits. Using well-characterized post-mortem brain samples, we explored the hypothesis that CA has lasting effects on the development of PNNs in the ventromedial PFC. We found that a history of CA was specifically associated with increased recruitment and maturation of PNNs. Through single-nucleus sequencing and fluorescent in-situ hybridization, we provide evidence for the involvement of oligodendrocyte progenitor cells (OPCs) in this phenomenon by showing that the expression of canonical components of PNNs are highly enriched and upregulated in this cell type in CA victims. These findings suggest that early-life adversity may lead to persistent patterns of maladaptive behaviours by reducing the neuroplasticity of cortical circuits through the enhancement of developmental OPC-mediated PNN formation.

Introduction

Child abuse (CA) has enduring effects on psychological development. Severe adversity during sensitive periods, during which personality traits, attachment patterns, cognitive functions and emotional responses are shaped by environmental experiences, is thought to have a profound effect on the structural and functional organization of the brain (1).

At the cellular level, childhood and adolescence are marked by the establishment and maturation of neural circuits. This protracted period is characterized by windows of heightened plasticity that precede the development of functional inhibitory connections and the balance of excitatory-inhibitory neurotransmission (2). A major mechanism behind the closing of these windows in neocortex is the recruitment of perineuronal nets (PNNs), a condensed form of extracellular matrix forming most notably around parvalbumin-expressing (PV+) interneurons. PNNs are thought to gradually decrease heightened plasticity by stabilizing the integration and function of PV+ cells into cortical networks and hindering the remodelling of these networks (3, 4). This PNN-induced stabilization of PV+ interneuron connectivity has been notably linked to the persistence of long-term associations, including fear memories (5–7).

Although little is known regarding the cellular effects of CA, evidence in rodents suggests that early-life stress associates with precocious functional maturation of PV+ neurons and the early emergence of adult-like characteristics of fear and extinction learning (8), in addition to discrete changes in the immunoreactivity of inhibitory neuron markers and PNNs (9). Taken together, these observations suggest that CA may alter the formation of PNNs.

We addressed this question using well-characterized post-mortem samples (Douglas-Bell Canada Brain Bank) from adult depressed suicides who died during an episode of major depression with (DS-CA) or without (DS) a history of severe child abuse and from matched psychiatrically healthy individuals (CTRL). Standardized psychological autopsies were conducted to provide comprehensive post-mortem diagnostic and retrieve various dimensions of childhood experience, including history and severity of CA. We focused on the ventromedial prefrontal cortex (vmPFC), a brain area closely linked to emotional learning and which is structurally and functionally altered in individuals with a history of CA (1).

Results and discussion

PNNs densities, visualized by Wisteria Floribunda Lectin (WFL) labeling and NeuN immunostaining (**Fig.1A**) were markedly higher in the vmPFC of individuals with a history of CA (**Fig.1B**). To understand whether these changes were directly linked to increased PNNs recruitment rather than changes

in PV+ cells numbers, we compared ratios of PV+ cells surrounded by PNNs. PV antigenicity is particularly susceptible to freezing, and lost altogether in samples snap frozen prior to fixation. We therefore developed an approach to combine fluorescence in-situ hybridization (FISH) and immunofluorescence to visualize PVALB expressing cells and PNNs in frozen samples (**Fig.1C**). ~65% of PVALB+ cells were surrounded by PNNs (**Fig.1D**), in line with previous observations. Importantly, samples from DS-CA individuals displayed a robust increase in the percentage of PVALB+ cells surrounded by PNNs compared to DS and CTRL samples (**Fig.1D**).

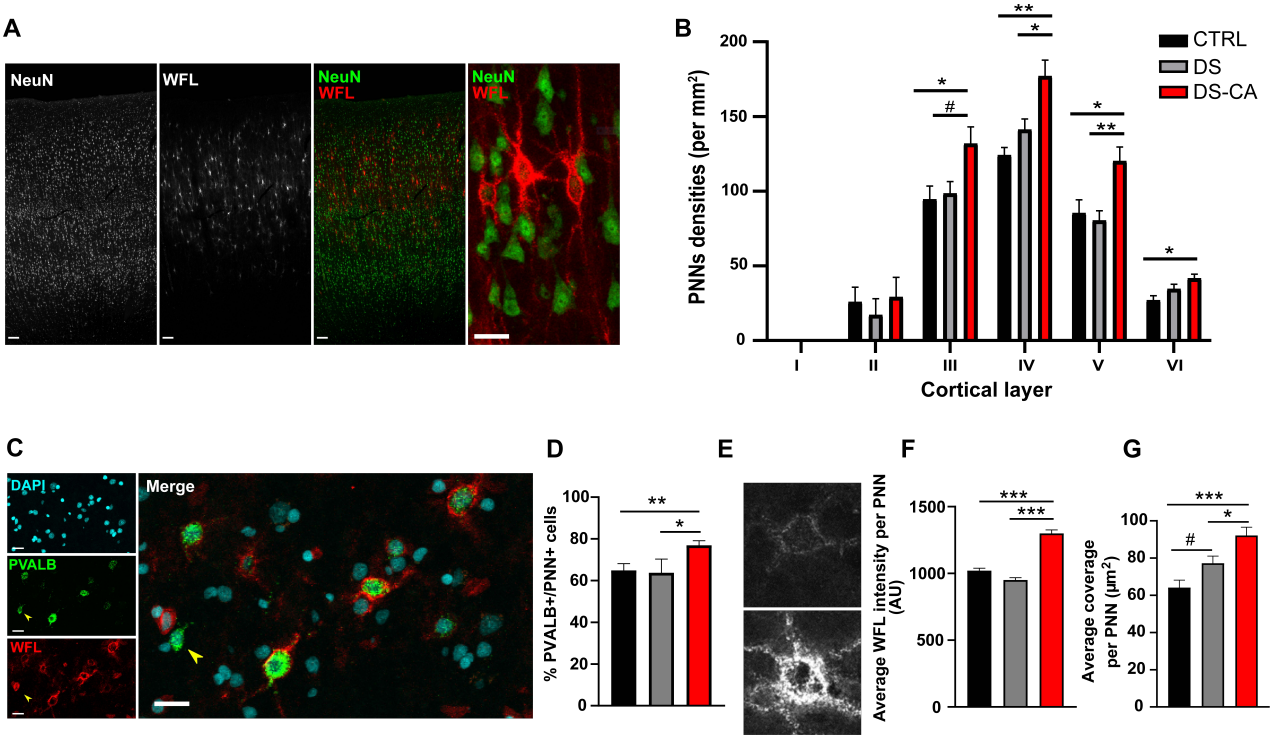

Figure 1. (**A**) Representative images of PNNs labeled with WFL and their distribution throughout the cortical layers of the human vmPFC. Scale bars = 100 and 20 µm (high magnification panel) (**B**) Depressed suicides with a history of child abuse (DS-CA, N = 11) have significantly higher densities of PNNs compared to controls (CTRL, N = 10) and depressed suicides without history of child abuse (DS, N= 14) (layer x group: F (10, 115) = 2.07, P< 0.05, followed by Tukey's multiple comparisons test: *: P<0.05, **: P<0.01, #:P< 0.10). (**C**) Representative images of in situ hybridization for PVALB (green) followed by WFL labeling (red). Nuclei were stained with DAPI (cyan). Yellow arrowhead points to a PVALB+/PNN- cell. Scale bars = 25µm. (**D**) DS-CA (N=9) subjects have higher ratios of PVALB+ cells surrounded by PNNs compared to CTRLs (N =8) and DS subjects (N=4) (Kruskal-Wallis ANOVA H(2,21) = 9.45, P<0.01, followed by Dunn's test for two by two comparisons: **:P<0.01, *:P<0.05). (**E**) Representative images of a low (top) and high (bottom) intensity PNN in the vmPFC. (**F**) PNNs from DS-CA subjects (N=475; 6) showed higher average WFL intensity compared to CTRLs (N= 387; 6) or DS (N=479; 5). One-way ANOVA: F(2, 1338) = 80.56, P<0.001, followed by Tukey's multiple comparisons test: ***:P<0.001. (**G**) PNNs from DS-CA subjects (N=432; 6) showed higher complexity (area covered by PNNs) compared to CTRLs (N= 363; 6) or DS (N=467; 5). One-way ANOVA: F (2, 1259) = 11.06, P<0.001, followed by Tukey's multiple comparisons test: ***:P<0.001, *:P<0.05, #:P<0.1.

Since other features could reflect maturational changes of PNNs associated with CA, we compared the intensity of WFL staining between groups (**Fig.1E**) as an indication of their maturity (10), as well as the area covered by individual PNNs as an indicator of their morphological complexity. CA was both associated with higher intensity of WFL staining per PNN (**Fig.1F**) and cells more extensively covered by PNNs (**Fig.1G**), suggesting overall that CA may precipitate both the maturation and the recruitment of PNNs around PV+ cells.

We then sought to explore the molecular underpinnings of this phenomenon, and reasoned that increased recruitment of PNNs associated with CA should translate or be induced by changes in the molecular programs controlling PNN assembly. Our understanding of these transcriptional programs is particularly scarce, hindered by the fact that several known molecules participating in PNN recruitment are released non-locally and by different cell types, implying a complex cellular crosstalk orchestrating PNN assembly. To gain insight into how, in humans, different cell types contribute to the synthesis of canonical components of PNNs, we explored a single-nucleus sequencing dataset previously generated by our group in the human PFC (11), and screened their expression across 8 major cell types. The main canonical components of PNNs, namely aggrecan, neurocan, versican, phosphacan, brevican, and tenascin-R, were highly enriched in oligodendrocyte progenitor cells (OPCs) (**Fig.2A**). This was further validated using FISH (**Fig.2B and 2C**) for versican (VCAN) and phosphacan (PTPRZ1), as they showed the strongest expression in OPCs and are two major signature genes in late OPCs (12). We found that virtually all PDGFRA+ OPCs express high levels of these components, while cells expressing these genes are almost all PDGFRA+ OPCs (**Fig.2D and 2E**). This strongly suggests that OPCs are likely potent regulators of PNN formation, as they are also ontogenetically-related to PV+ cells (13) and have been shown to form extensive synaptic networks with them (14).

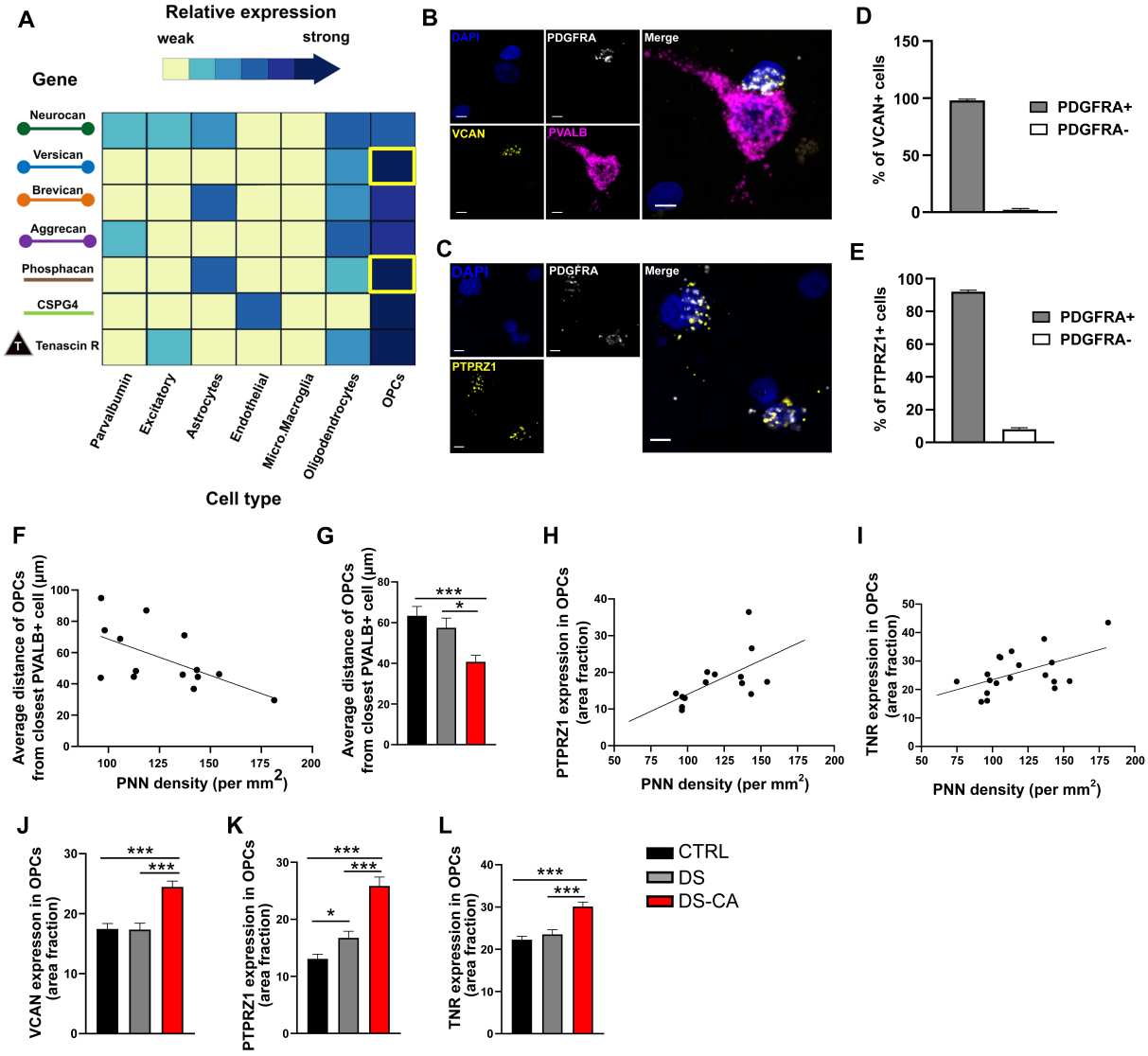

Figure 2. (A) Average gene expression of canonical components of PNNs according to cell type, derived from single-nucleus sequencing of human prefrontal cortex samples from 5 control subjects (11). Expression was calculated by weighting normalized transcript counts of each cluster by the size (number of nuclei) of the cluster. Weighted average expression values are displayed in a heatmap, with the expression values as z-scores, and darker colors indicating higher expression. OPCs consistently express higher levels of most of these components compared to other cell types. (**B**) Representative images of in situ hybridization validation of VCAN (Versican, yellow) expression in OPCs (PDGFRA+ cells, white). Note the VCAN expressing OPC directly juxtaposed to a PVALB+ (magenta) cell. Nuclei were counterstained with DAPI (blue). Scale bar = 5 µm. (**C**) Representative images of in situ hybridization validation of PTPRZ1 (Phosphacan, yellow) expression in OPCs (PDGFRA+ cells, white). Nuclei were counterstained with DAPI (blue). Scale bar = 5 µm. (**D-E**) Both VCAN (**D**) and PTPRZ1 (**E**) expression is highly enriched in OPCs, with 97.8 percent of VCAN+ cells (N=225) co-expressing PDGFRA (**D**), and 91.8 percent of PTPRZ1+ cells (N= 281) co-expressing PDGFRA (**E**). (**F**) A negative correlation was found between average distance of OPCs from closest PVALB+ cell and PNNs density (R^2 = 0.36, P<0.05) in the same subjects, suggesting that OPCs proximity with PVALB+ cells could reflect changes in PNN density. (**G**) Proximity of OPCs with PVALB+ cells was decreased in DS-CA subjects (N=90 OPCs, 5 subjects) compared to CTRLs (N= 106 OPCs, 6 subjects) and DS (N= 73 OPCs, 4 subjects) (One-way ANOVA: F (2, 266) = 7.963, P<0.001, followed by Tukey's multiple comparison test, ***:P<0.001, *:P<0.05). (**H-I**) Both PTPRZ1 (**H**) and TNR (**I**) average expression in OPCs modestly correlated with PNNs densities (R^2 = 0.35, P<0.05 and R^2 = 0.28, P<0.05 respectively). (**J**) The average expression of VCAN in OPCs was significantly higher in DS-CA subjects (N=139 cells, 7 subjects) compared to CTRLs (N= 160 cells, 8 subjects) and DS (N= 119 cells, 6 subjects) (One-way ANOVA F (2, 415) = 17.25, P<0.001, followed by Tukey's multiple comparisons test, ***:P<0.001). (**K**) The average expression of PTPRZ1 in OPCs was significantly higher in DS-CA subjects (N=63 cells, 4 subjects) compared to CTRLs (N= 117 cells, 6 subjects) and DS (N= 81 cells, 5 subjects) (One-way ANOVA F (2, 258) = 31.65, P<0.001, followed by Tukey's multiple comparisons test, ***:P<0.001, *:P<0.05). (**L**) The average expression of TNR in OPCs was significantly higher in DS-CA subjects (N=200 cells, 8 subjects) compared to CTRLs (N= 207 cells, 7 subjects) and DS (N= 160 cells, 5 subjects) (One-way ANOVA, F (2, 564) = 18.69, P<0.001, followed by Tukey's multiple comparisons test, ***:P<0.001).

OPCs were on occasions found to be directly juxtaposed to PVALB+ cells (**Fig.2B**), as previously reported in rodents (15). Interestingly, OPC proximity to PVALB+ cells modestly correlated with PNN density (**Fig.2F**), and was increased in individuals with a history of CA (**Fig.2G**), further suggesting an interplay between these two cell types. In support of a possible involvement of OPCs in mediating CA-related changes in PNNs, the expression of both PTPRZ1 and TNR in OPCs correlated with PNNs densities (**Fig.2H and 2I**) and were upregulated in OPCs of CA victims (**Fig.2J-L**).

Overall, our results suggest that a history of CA associates with increased recruitment and maturation of PNNs, as well as an upregulation of their canonical components by OPCs, a cell type that likely plays a key role in the cellular crosstalk that orchestrates PNN formation. Whether changes in OPCs are causal in the increased recruitment of PNNs following CA or an indirect response following changes in PNN dynamics remains to be explored in preclinical models. These findings raise the possibility that aversive memories and maladaptive patterns of emotional processing associated with early-life adversity could be stabilized more durably in the brain of CA victims, thus favoring the emergence of psychopathologies.

Acknowledgments

The present study used the services of the Douglas-Bell Canada Brain Bank and of the Molecular and Cellular Microscopy Platform (MCMP) at the Douglas Hospital Research Centre. The authors are grateful to Maâmar Bouchouka, Josée Prud'homme, Dominique Mirault, and Melina Jaramillo Garcia for their kind assistance.

Author Contributions

AT and NM conceived the study. GT participated in the acquisition and clinical characterization of the brain samples. AT, CB, FD, MAD, CC, RM contributed to immunohistological experiments. AT, CN, MM and KP generated and analysed the snSeq dataset. AT and FC performed the in situ hybridization experiments. AT and NM prepared the manuscript and all authors contributed to and approved its final version.

Competing Interest Statement

The authors have no financial interest or conflict of interest to declare.

Funding

This work was funded by a CIHR Project grant to NM. AT was supported by fellowships from the FRQS and Toronto Dominion, and an American Foundation for Suicide Prevention (AFSP) Young Investigator Innovation Grant (YIG-0-146-17). The Molecular and Cellular Microscopy Platform and the Douglas-Bell Canada Brain Bank (DBCBB) are partly funded by a Healthy Brains for Healthy Lives (CFREF) Platform Grant to GT and NM. The DBCBB is also funded by the Réseau Québécois sur le suicide, le troubles de l'humeur et les troubles associés (FRQS).

References

1. M. H. Teicher, J. a. Samson, C. M. Anderson, K. Ohashi, The effects of childhood maltreatment on brain structure, function and connectivity. *Nat. Rev. Neurosci.* **17**, 652–666 (2016).

2. B. R. Ferguson, W.-J. Gao, PV Interneurons: Critical Regulators of E/I Balance for Prefrontal Cortex-Dependent Behavior and Psychiatric Disorders. *Front. Neural Circuits* **12**, 37 (2018).

3. J. W. Fawcett, T. Oohashi, T. Pizzorusso, The roles of perineuronal nets and the perinodal extracellular matrix in neuronal function. *Nat. Rev. Neurosci.* (2019) https:/doi.org/10.1038/s41583-019-0196-3.

4. B. A. Sorg, *et al.*, Casting a wide net: Role of perineuronal nets in neural plasticity in *Journal of Neuroscience*, (Society for Neuroscience, 2016), pp. 11459–11468.

5. N. Gogolla, P. Caroni, A. Lüthi, C. Herry, Perineuronal nets protect fear memories from erasure. *Science (80-.).* **325**, 1258–1261 (2009).

6. E. H. Thompson, *et al.*, Removal of perineuronal nets disrupts recall of a remote fear memory. *Proc. Natl. Acad. Sci. U. S. A.* **115**, 607–612 (2018).

7. W. Shi, *et al.*, Perineuronal nets protect long-term memory by limiting activity-dependent inhibition from parvalbumin interneurons. *Proc. Natl. Acad. Sci. U. S. A.* (2019) https:/doi.org/10.1073/pnas.1902680116 (January 3, 2020).

8. K. Bath, G. Manzano-Nieves, H. Goodwill, Early life stress accelerates behavioral and neural maturation of the hippocampus in male mice. *Horm. Behav.* **82**, 64–71 (2016).

9. S. Murthy, *et al.*, Perineuronal Nets, Inhibitory Interneurons, and Anxiety-Related Ventral Hippocampal Neuronal Oscillations Are Altered by Early Life Adversity. *Biol. Psychiatry* **85**, 1011–1020 (2019).

10. Y. M. Sigal, H. Bae, L. J. Bogart, T. K. Hensch, X. Zhuang, Structural maturation of cortical perineuronal nets and their perforating synapses revealed by superresolution imaging. *Proc. Natl. Acad. Sci. U. S. A.* **116**, 7071–7076 (2019).

11. C. Nagy, *et al.*, Single-nucleus transcriptomics of the prefrontal cortex in major depressive disorder implicates oligodendrocyte precursor cells and excitatory neurons. *Nat. Neurosci.* **23**, 771–781 (2020).

12. K. Perlman, *et al.*, Developmental trajectory of oligodendrocyte progenitor cells in the human

brain revealed by single cell RNA sequencing. *Glia* **68**, 1291–1303 (2020).

13. D. Orduz, *et al.*, Developmental cell death regulates lineage-related interneuron-oligodendroglia functional clusters and oligodendrocyte homeostasis. *Nat. Commun.* **10**, 4249 (2019).

14. D. Orduz, *et al.*, Interneurons and oligodendrocyte progenitors form a structured synaptic network in the developing neocortex. *Elife* **2015**, 1–53 (2015).

15. J. J. Boulanger, C. Messier, Oligodendrocyte progenitor cells are paired with GABA neurons in the mouse dorsal cortex: Unbiased stereological analysis. *Neuroscience* **362**, 127–140 (2017).

Material and Methods

Human post-mortem brain samples. Brain samples were obtained from the Douglas-Bell Canada Brain Bank (Montreal, Canada). Phenotypic information was retrieved through standardized psychological autopsies, in collaboration with the Quebec Coroner's Office and with informed consent from next of kin. Presence of any or suspected neurological/neurodegenerative disorder signalled in clinical files constituted an exclusion criterion. Cases and controls are defined with the support of medical charts and Coroner records. Proxy-based interviews with one or more informants best acquainted with the deceased are supplemented with information from archival material obtained from hospitals, Coroner's office and social services. Clinical vignettes are then produced and assessed by a panel of clinicians to generate DSM-IV diagnostic criteria, providing sociodemographic characteristics, social developmental history, DSM-IV axis I diagnostic information and behavioural traits; information that is obtained through different adapted questionnaires. Toxicological assessments and medication prescription are also obtained. Presence of severe child abuse was based on adapted Childhood Experience of Care and Abuse (CECA) interviews assessing various dimensions of childhood experience, including abuse (Bifulco et al., 1994).

Table 1. Subjects characteristics

	CTRL	DS-CA	DS
N	11	12	16
Axis 1 diagnosis	0	MDD (11); DD-NOS (1)	MDD (14); DD-NOS (2)
Age (years)	43.18 ± 7.11	37.75 ± 3.10	46.63 ± 3.48
Sex (M/F)	9/2	9/3	14/2
PMI (hours)	35.95 ± 7.15	40.92 ± 6.68	45.95 ± 8.06
Tissue pH	6.4 ± 0.09	6.56 ± 0.08	6.52 ± 0.07
Substance dependence	0	5	6
Medication	0	SSRI (2); Benzodiazepines (2); Antipsychotics (1); Antimanic (1)	SSRI (4); SNRI (1); TCA antidepresants (1); Benzodiazepines (3); Antipsychotics (2); Antimanic (1)

Data represent mean ± s.e.m. PMI: Post-mortem interval; MDD: Major Depressive Disorder; DD-NOS: Depressive Disorder Not Otherwise Specified. SSRI: Selective Serotonin Reuptake Inhibitor; SNRI: Selective Norepinephrine Reuptake Inhibitor; TCA: tricyclic antidepressant.

Tissue dissections

Dissections were performed by expert brain bank staff on fresh-frozen 0.5 cm thick coronal sections with the guidance of a human brain atlas. Ventromedial prefrontal cortex samples were dissected in sections equivalent to plate 3 (approximately − 48 mm from the center of the anterior commissure) of this atlas. Samples were either kept frozen or fixed overnight in 10% formalin until processed for in situ hybridization or immunohistochemistry, respectively.

Immunohistochemistry

Frozen tissue blocks were fixed in 10% neutral buffered formalin overnight at 4 °C, rinsed in PBS and kept in 20% sucrose/PBS solution until serially sectioned at 40 µm on a cryostat. Free-floating sections

were rinsed in phosphate-buffered saline (PBS) and then incubated overnight at 4ºC under constant agitation with a mouse anti-NeuN antibody (Millipore, 1:500, MAB377) and biotinylated Wisteria Floribunda Lectin (WFL, Vector Laboratories, B-1355; 1:2500) diluted in a blocking solution of PBS/0.2% Triton-X/2% normal donkey serum. Sections were then rinsed and incubated for 2h at room temperature with Cy3-conjugated Streptavidin (Jackson ImmunoResearch, 016-160-084; 1:500) for the detection of PNNs and Alexa-488 conjugated anti-Mouse (Jackson ImmunoResearch, 1:500) for NeuN, diluted in the same blocking solution as the primary incubation. Following the secondary antibody incubation, sections were rinsed, endogenous autofluorescence from lipofuscin and cellular debris was quenched with Trueblack (Biotium), and sections were mounted on Superfrost charged slides and coverslipped with Vectashield mounting medium (Vector Laboratories, H-1800).

Whole vmPFC sections were scanned on a Zeiss Axio Imager M2 microscope equipped with a motorized stage and Axiocam MRm camera at x20. The ImageJ software (NIH) Cell Counter plugin was used to manually count PNNs. An average of 4 sections per subject was used. Cortical layers were delineated based on NeuN+ cells distribution and morphology, and the number of PNNs as well as the area of each layer were measured, allowing to generate PNNs density values (n/mm²).

Fluorescent in situ hybridization

Frozen BA9 blocks were cut serially with a cryostat and 10µm-thick sections collected on Superfrost charged slides. In situ hybridization was performed using Advanced Cell Diagnostics RNAscope® probes and reagents following the manufacturer instructions. Sections were first fixed in cold 10% neutral buffered formalin for 15 minutes, dehydrated by increasing gradient of ethanol bathes and air dried for 5 minutes. Endogenous peroxidase activity was quenched with hydrogen peroxide for 10 minutes followed by protease digestion for 30 min at room temperature. The following probes were then hybridized for 2 hours at 40C in a humidity-controlled oven: Hs-PVALB (cat. no. 422181), Hs-VCAN (cat. no. 430071-C2), Hs-PDGFRA (cat. no. 604481-C3), Hs-TNR (cat. no. 525811), Hs-PTPRZ1 (cat. no. 584781-C2). Amplifiers were added using the proprietary AMP reagents, and the signal visualized through probe-specific HRP-based detection by tyramide signal amplification with Opal dyes (Opal 520, Opal 570 or Opal 690; Perkin Elmer) diluted 1:700. Slides were then coverslipped with Vectashield mounting medium with DAPI for nuclear staining (Vector Laboratories) and kept at 4C until imaging. For immunohistochemical staining of PNNs following PVALB in situ hybridization, slides were rinsed in PBS, incubated overnight at 4C with biotinylated WFL followed by Cy3-conjugated Streptavidin for 2 hours prior to coverslipping.

Imaging and analysis of in situ RNA expression in OPCs

Image acquisitions was performed on a FV1200 laser scanning confocal microscope (FV1200) equipped with a motorized stage. For each experiment and subject, 6 to 10 stack images were taken to capture at least 20 OPCs (PDGFRA+) per subject. Images were taken using a x60 objective (NA = 1.42) with a XY pixel width of ~0.25µm and Z spacing of 0.5µm. Laser power and detection parameters were kept consistent between subjects for each set of experiment. Since TSA amplification with Opal dyes yields a high signal to noise ratio, parameters were optimized so that autofluorescence from lipofuscin and cellular debris was filtered out. OPCs were defined by bright clustered puncta-like PDGFRA signal present within the nucleus of the cells. Using ImageJ, stacks were first converted to Z-projections, and for each image the nuclei of OPCs were manually contoured based on DAPI expression. Expression of VCAN, TNR or PTPRZ1 in OPCs was quantified using the area fraction, whereby for each probe the signal was first manually thresholded and the fraction of the contoured nucleus area covered by signal measured for each OPC. Area fraction was the preferred measure to reflect RNA expression as punctate labeling

generated by FISH often aggregates into clusters that cannot readily be dissociated into single dots or molecules.

Ratios of PVALB+/PNN+ cells

Proportions of PVALB+ cells enwrapped by PNNs were determined in a single section. An average of 55 PVALB+ cells per subject were imaged under a x20 objective through layers 4-5 of the vmPFC.

Intensity and area measurements

For each subject, ~15 z-stacks (0.26µm Z-spacing) spanning all layers of the vmPFC were acquired at 40x magnification on an Olympus FV1200 laser scanning confocal microscope. PNNs were traced manually with ImageJ using maximum intensity projections generated from each stack. For each PNN, the mean pixel value of adjacent background was subtracted to the mean pixel value of the contoured soma of the PNN, yielding the mean corrected fluorescence intensity. To infer on their morphological complexity, we measured the area covered by each contoured PNN, including soma and ramifications extending over proximal dendrites.

Cell-type specific expression of PNN canonical components using single-nucleus sequencing

Cell-type specific expression of canonical components of PNNs was explored using a snRNA-seq dataset from the human prefrontal cortex previously generated by our group (11), for which methodology is extensively described in this published resource. Average expression for each PNN component in each cell type was calculated by weighting the expression values (normalized transcript counts) of each cluster by the size (number of nuclei) of the cluster. Weighted average expression values are displayed in a heatmap, scaled by row (i.e. gene). The color bar therefore represents the expression values as z-scores, with darker colors indicating higher expression.

Statistical analyses

Analyses were performed on Statistica version 12 (StatSoft) and Prism version 6 (GraphPad Software). Distribution and homogeneity of variances were assessed with Shapiro–Wilk and Levene's tests, respectively. PNNs densities were analyzed using a mixed-effects model, using layer and group as fixed factors, followed by Tukey's HSD test for corrected post hoc comparisons. For all other variables (WFL intensity, WFL area per PNN, PNN+/PVALB ratios, RNA expression in OPCs and distance of OPCs from PVALB+ cells) group effects were detected using one-way ANOVAs or Kruskal-Wallis test followed by Tukey's HSD or Dunn's test respectively. Linear regressions were used to address the relationship between PNNs densities, distance of OPCs from PVALB+ cells, and RNA expression of canonical components of PNNs. Significance threshold was set at 0.05.